THE JOURNAL OF PHYSICAL CHEMISTRY C

Article

Cite This: J. Phys. Chem. C 2018, 122, 7494−7503

pubs.acs.org/JPCC

Chemical Vapor Deposition Synthesis of MoS_2 Layers from the Direct Sulfidation of MoO_3 Surfaces Using Reactive Molecular Dynamics Simulations

Sungwook Hong,[†] Chunyang Sheng,[†] Aravind Krishnamoorthy,[†] Pankaj Rajak,[†] Subodh Tiwari,[†] Ken-ichi Nomura,[†] Masaaki Misawa,[†,‡] Fuyuki Shimojo,[‡] Rajiv K. Kalia,[†] Aiichiro Nakano,[†] and Priya Vashishta*[,†]

[†]Collaboratory for Advanced Computing and Simulations, Department of Physics & Astronomy, Department of Computer Science, Department of Chemical Engineering & Materials Science, and Department of Biological Sciences, University of Southern California, Los Angeles, California 90089-0242, United States

[‡]Department of Physics, Kumamoto University, Kumamoto 860-8555, Japan

Supporting Information

ABSTRACT: Atomically thin MoS_2 layer, a promising transition metal dichalcogenide (TMDC) material, has great potential for application in next-generation electronic and optoelectronic devices. Chemical vapor deposition (CVD) is the most effective technique for the synthesis of high-quality MoS_2 layers. During CVD synthesis, monolayered MoS_2 is generally synthesized by sulfidation of MoO_3. Although qualitative reaction mechanisms for the sulfidation of MoO_3 have been investigated by previous studies, the detailed reaction processes, including atomic-scale reaction pathways and growth kinetics, have yet to be fully understood. Here, we present quantum-mechanically informed and validated reactive molecular dynamics simulations of the direct sulfidation of MoO_3 surfaces using S_2 gas precursors. Our work clarifies the reaction mechanisms and kinetics of the sulfidation of MoO_3 surfaces as follows: the reduction and sulfidation of MoO_3 surfaces occur primarily at O-termination sites, followed by unsaturated Mo sites; these local reaction processes lead to nonuniform MoO_xS_y surface structures during the CVD process. After annealing the MoO_xS_y samples, the crystallized surface structures contain voids, and three different types of local surface complexes (MoO_x, MoO_xS_y, and MoS_2-like surface regions), depending on the fraction of S ingredients on the MoO_xS_y surface. These results, which have been validated by our reactive quantum molecular dynamics simulations and previous experimental results, provide valuable chemical insights into the CVD synthesis of large-scale and defect-free MoS_2 layers and other layered TMDC materials.

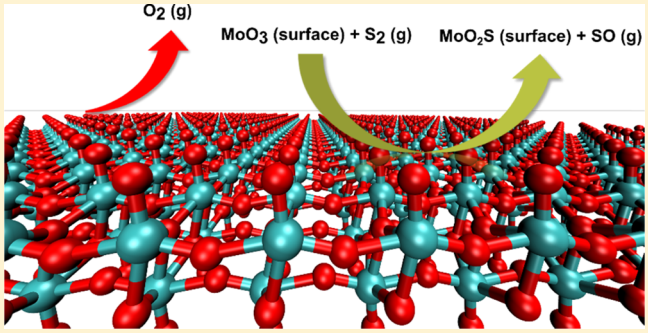

1. INTRODUCTION

Two-dimensional and layered materials such as graphene, transition metal dichalcogenide (TMDC), and hexagonal boron nitride have gained more attention for the exploration of functional nanostructures.[1−3] In particular, MoS_2 monolayer is a promising semiconducting TMDC material with great potential for electronic applications due to its outstanding physical and chemical properties, such as a layer-dependent band gap, high carrier mobility, and strong absorption in the visible frequencies.[4−9] Atomically thin MoS_2 layer has also been found to possess exceptional mechanical properties, applicable to flexible devices.[10] To bring such a fascinating mono/few MoS_2 layer into mass production, a wide range of synthesis techniques for MoS_2 layers and other layered TMDC materials has been proposed and developed, including mechanical exfoliation, physical vapor deposition, hydrothermal synthesis, and chemical vapor deposition (CVD).[11−13]

Among these techniques, CVD is the most effective method for synthesizing atomically thin MoS_2 layers on substrates because of its low cost, simplicity, uniformity, and scalability, compared with the other methods.[13] During CVD synthesis of MoS_2 layers, MoO_3 reactants and gas-phase sulfur precursors are generally used.[14,15] Thus, understanding the chemical reactions of MoO_3 reactants and gas-phase sulfur precursors is essential for the CVD synthesis of large-scale and defect-free MoS_2 layers. For this reason, numerous efforts have been made to investigate the reaction mechanisms during the CVD synthesis of MoS_2 layers.[16−20] Consequently, qualitative reaction mechanisms for the CVD synthesis of MoS_2 layers have been generally understood as follows: (a) the MoO_3 reactant is vaporized and interacts with gas-phase sulfur

Received: December 6, 2017
Revised: March 8, 2018
Published: March 9, 2018

DOI: 10.1021/acs.jpcc.7b12035
J. Phys. Chem. C 2018, 122, 7494−7503

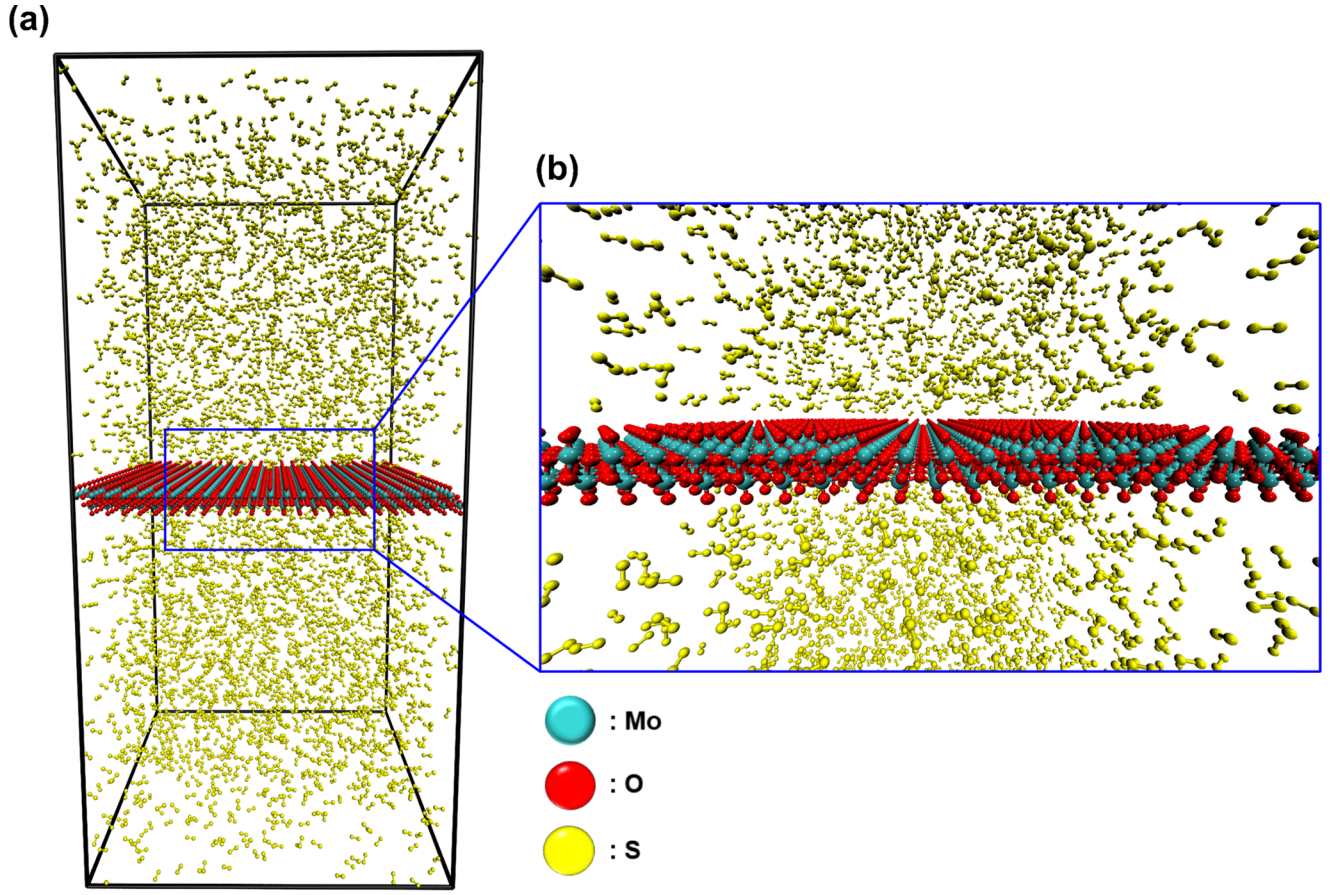

Figure 1. (a) Initial configuration of a monolayered MoO_3 surface (4608 atoms) with 4000 S_2 gas molecules (8000 atoms) for RMD simulations (within an orthogonal cell of 94.18 Å × 91.14 Å × 200.0 Å). (b) Closeup of the MoO_3 surface interacting with the S_2 gas environment. During the RMD simulations, S_2 molecules react with the MoO_3 surface, leading to reduction and sulfidation steps.

precursors in CVD chambers, leading to molybdenum oxysulfide (Mo-oxysulfide) intermediates; (b) during further reaction processes, the Mo-oxysulfide intermediates convert into MoS_2 entities; and (c) the MoS_2 entities are finally deposited onto substrates and merged into continuous MoS_2 layers. Furthermore, recent experimental studies[20,21] have suggested that using the as-deposited MoO_3 surface on the substrates, instead of vaporized MoO_3 powders, could lead to a high uniformity of MoO_2 layers during CVD synthesis. During this approach, the as-deposited MoO_3 surface most likely reacts with sulfur precursors on its surface, finally transforming into MoS_2 layers. As such, it is expected that the direct sulfidation of MoO_3 surfaces is a key reaction event during the CVD process.

However, the detailed reaction pathways for the sulfidation of MoO_3 surfaces have yet to be fully investigated. In addition, the reaction kinetics for the sulfidation of MoO_3 surface remains unclear. These shortcomings are primarily due to the lack of experimental devices that capture these complex reaction events (i.e., short time scales and limited spatial resolution).[22] Atomistic modeling and simulations enable us to study dynamic behaviors of complex materials at the atomic level.[23,24] Particularly, reactive molecular dynamics (RMD) simulations allow one to describe reactive events, thus providing valuable information on the chemical and physical properties of nanoscale systems.[25−27]

Here, we present quantum-mechanically informed and validated ReaxFF[28]-RMD simulations of the direct sulfidation of MoO_3 surfaces using S_2 gas precursors to clarify key reaction events during the CVD synthesis of MoS_2 layers. To validate the critical reaction steps described by our RMD simulations, we also performed quantum molecular dynamics (QMD) simulations for the reactions of reduced MoO_3 flakes and S_2 molecules and compared the results of RMD simulations to those of previous experimental studies. Our goal is to obtain a better understanding of atomic-scale CVD synthesis processes of MoS_2 monolayers and other TMDC materials. In this work, we provide new chemical insights into the mechanisms of the direct sulfidation of MoO_3 surfaces and the reaction kinetics during the sulfidation and postannealing processes of the MoO_3 surface.

2. METHODS

To describe the full dynamics of complex systems including chemical reactions, empirical reactive potentials or force fields such as COMB[29,30] and ReaxFF[28] can be effectively used and coupled with large-scale RMD simulations.[31] Especially, ReaxFF has shown its ability of successfully predicting not only gas-surface reactions[32−34] but also characteristics of two-dimensional materials.[35−39] A recent review paper[40] has provided further information on the ReaxFF potential and its applications. In this work, we used ReaxFF reactive force-field parameters for Mo/O/S elements that we previously reoptimized and validated for the CVD synthesis of MoS_2 layers.[41] ReaxFF reactive force-field parameters used in this study can be found in the Supporting Information. To control system temperatures during RMD simulations, the NVT

DOI: 10.1021/acs.jpcc.7b12035
J. Phys. Chem. C 2018, 122, 7494−7503

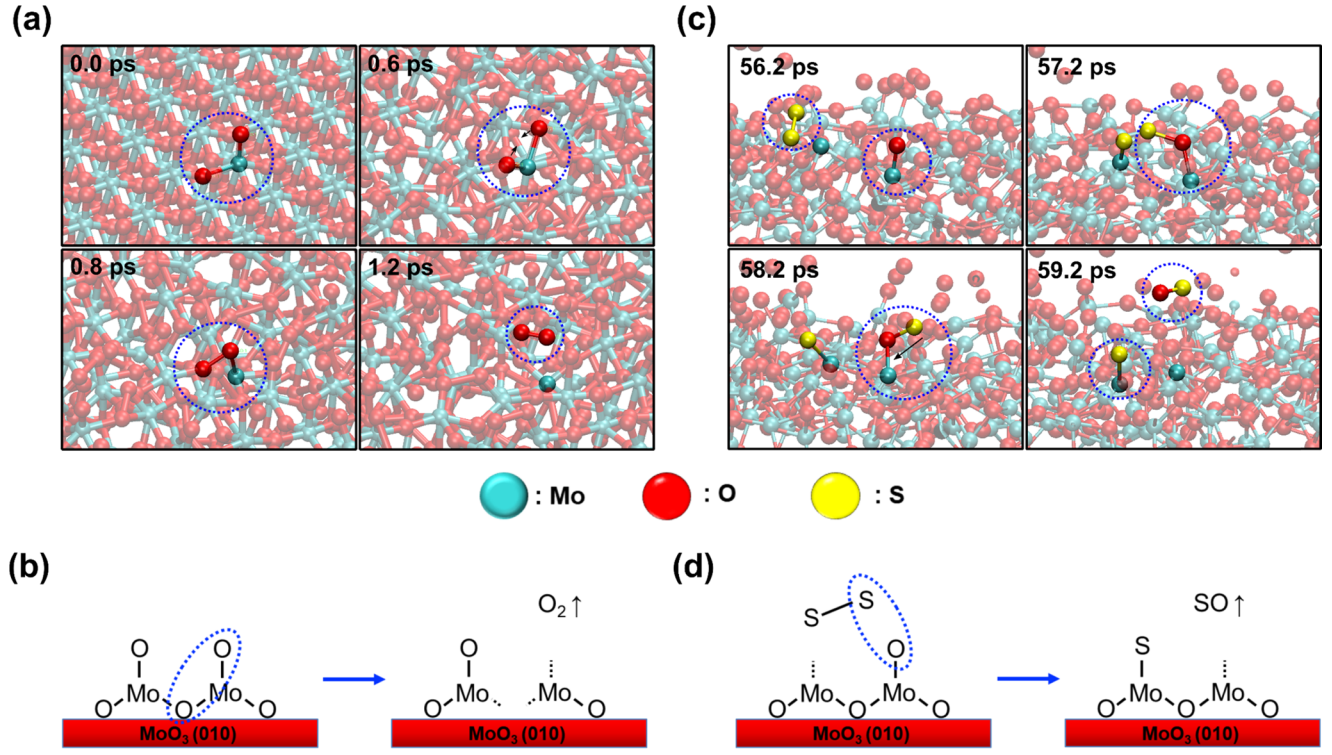

Figure 2. Reaction mechanisms for reduction and sulfidation processes of the MoO_3 surface described by RMD simulations. (a) RMD trajectories of the reduction process at 3000 K. The MoO_3 surface is reduced primarily by breaking Mo−O bonds: one from the O-termination site and the other from the Mo−O−Mo bridge, liberating an O_2 molecule. (b) Schematics of the reaction mechanism for the reduction process in (a). (c) RMD trajectories of the sulfidation process at 3000 K. S_2 molecule reacts preferably with an O-termination site, along with a neighboring Mo-dangling bond, resulting in the formation of Mo−S bond and SO gas molecule. (d) Schematics of the reaction mechanism of the sulfidation process in (c). Note that the blue dotted circles and black arrows in (a, c) highlight local surface composition/molecules and critical reaction steps (i.e., bond breakage or formation), respectively. The blue dotted ellipses in (b, d) represent atoms in the surface structure and/or gas molecules participating in the key reaction steps.

ensemble with the Nosé−Hoover[42,43] thermostat was applied to the whole systems; a relatively small time step of 0.20 fs along with a temperature damping constant of 20.0 fs was used to properly describe chemical reactions for our RMD simulations. During the sulfidation process, we used an orthogonal cell of 94.18 Å × 91.14 Å × 200.0 Å, which included a monolayered MoO_3 surface (94.18 Å × 91.14 Å × 6.0 Å) in the middle of the cell and 4000 S_2 gas molecules (system density: 0.42 g/cm^3). In addition, a periodic boundary condition was applied to all of the directions. Then, the entire system was exposed to 3000 K for 2.0 ns, followed by 4000 K for 1.8 ns and 5000 K for 2.0 ns. Note that our simulated temperatures (3000−5000 K) were much higher than the experimental temperatures (~1200 K)[13,15] so that the MoO_3 surface was easily vaporized, thus not holding solid-phase MoO_xS_y surface structures during the RMD simulations. For this reason, one-body spring forces were independently applied to all of the Mo atoms in the MoO_3 surface. In doing so, we could successfully describe key reaction events during our RMD simulations (such as O_2/SO gas and Mo−S bond formation) while preventing diffusion of Mo atoms into vacuum layers (i.e., the system kept maintaining solid-phase MoO_xS_y surface structures during the entire RMD simulations up to 5000 K). After that, we performed the annealing process of the reduced/sulfidized MoO_xS_y surfaces. For comparison, two different surface structures—$MoO_{0.69}S_{1.52}$ and $MoO_{0.42}S_{1.95}$ surfaces—were taken from the previous sulfidation processes at 3.8 and 5.8 ns, respectively. All of the gas-phase molecules in the vacuum layers were removed from these two simulation domains, and then, the surface structures were heated at a constant temperature of 1500 K up to 0.25 ns and cooled to 300 K for an additional 0.25 ns.

3. RESULTS AND DISCUSSION

Our work elucidates the detailed reaction pathways and kinetics for the sulfidation of MoO_3 surfaces. In this section, we report the results of our RMD and QMD simulations and their analyses.

3.1. Reaction Mechanisms for the Sulfidation of MoO_3 Surfaces. To clarify the reaction mechanisms associated with CVD synthesis of MoS_2 layers, we performed RMD simulations of the sulfidation process with a gas-surface system, including a monolayered MoO_3 surface (94.18 Å × 91.14 Å × 6.00 Å) and S_2 gas molecules (see Figure 1a,b).

Note that the system configuration is a simplified experimental model that uses as-deposited MoO_3 surfaces on substrates and vaporized sulfur precursors during the CVD process,[20,44] and we assumed that the reactions in the interface between as-deposited MoO_3/substrates do not play a critical role in the sulfidation of the MoO_3 surface. That is, our system only includes monolayered MoO_3 without supported substrates, interacting directly with S_2 gas molecules on the top and bottom surfaces. In doing so, we primarily simulated and investigated reaction events between the MoO_3 surface and S_2 gas molecules, leading to reduction and sulfidation steps efficiently. The system was then exposed to 3000 K for up to

DOI: 10.1021/acs.jpcc.7b12035
J. Phys. Chem. C 2018, 122, 7494−7503

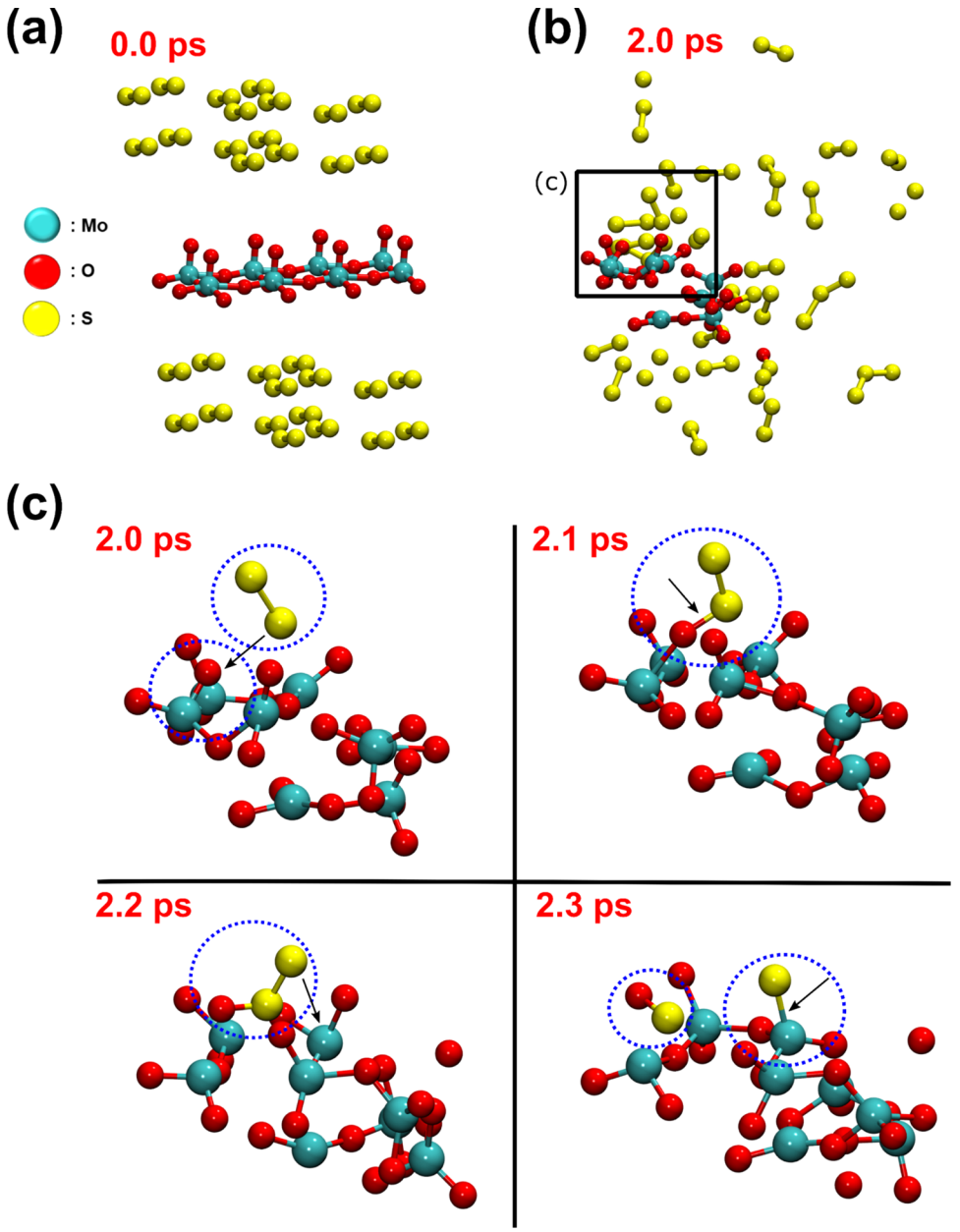

Figure 3. QMD simulations of the sulfidation of a reduced MoO_3 flake. System configurations (a) at 0.0 ps and (b) 2.0 ps. Note that the reduced MoO_x slab was vaporized at high temperature, thus accelerating the chemical reactions of the MoO_x and S_2 molecules. (c) Closeups of the black rectangle in (b) up to 2.3 ps, showing the reaction pathways for the sulfidation of the MoO_x cluster. The reaction mechanism by QMD simulation, leading to Mo−S bond and SO gas molecules, is in excellent agreement with our RMD simulations (see Figure 2c,d), thus validating our ReaxFF reactive force field for CVD simulations. The blue dotted circles and black arrows indicate critical reaction steps for the Mo−S bond and SO gas formation.

2.0 ns during our RMD simulations. It should also be noted that in our recently published work,[41] we suggested reaction mechanisms that are validated by the experimental literature,[16,45] for the reduction and sulfidation processes of MoO_3 surfaces involving (1) O_2 evolution, (2) SO/SO_2 formation, and (3) Mo−S bond formation. To further clarify our proposed reaction mechanisms, we investigated detailed RMD trajectories and the corresponding schematics of the reaction mechanisms that clearly show stepwise O_2 evolution.

Figure 2a−d demonstrates the reaction mechanisms for the reduction and sulfidation processes described above by taking into account detailed RMD trajectories. In Figure 2a, our RMD trajectories elucidate the reaction mechanism for the reduction process of the MoO_3 surface as follows: at 0.6 ps, the O atom in an O-termination site reacted preferably with a neighboring O atom in the Mo−O−Mo bridge; at 0.8 ps, the Mo−O bond in the Mo−O−Mo bridge broke, forming an O−O bond; at 1.2 ps, O_2 molecules desorbed for the MoO_3 surface, and thus, the surface was reduced. Figure 2b provides the schematics of this reaction mechanism, corresponding to the reduction step of the MoO_3 surface. It is worth noting that the reduction process described by our RMD simulation is in excellent agreement with X-ray photoemission spectroscopy experiments by Salazar et al.,[44] who confirmed that during the annealing process, the as-deposited MoO_3 surface was gradually reduced by Mo−O bond ruptures (i.e., the as-deposited MoO_3 surface lost O

DOI: 10.1021/acs.jpcc.7b12035
J. Phys. Chem. C 2018, 122, 7494−7503

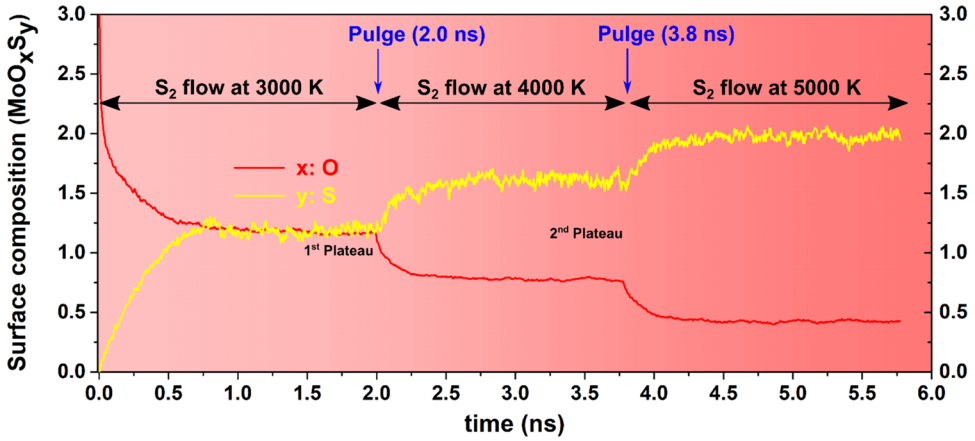

Figure 4. Rate of the reduction/sulfidation processes. Red and yellow curves represent a decrease in O atoms (i.e., reduction) and an increase in S atoms (i.e., sulfidation) on the MoO_xS_y surface composition, respectively, as a function of time. To increase the reaction rate, RMD simulations were performed at 3000 K for 2.0 ns, followed by 4000 K for 1.8 ns and then 5000 K for an additional 2.0 ns, and purging processes were performed at 2.0 and 3.8 ns.

atoms), thus validating our proposed reaction mechanism for the reduction step.

Subsequently, as shown in Figure 2c, S_2 gas molecule interacted with both the O-termination and O-vacancy site (at 56.2 and 57.2 ps), thus breaking the S−S bond and leading to Mo−S bond and SO gas molecule (at 58.2 and 59.2 ps); the reaction mechanisms for this sulfidation process are also summarized in Figure 2d. To validate the full dynamics of our RMD simulations for the Mo−S bond and SO gas formation at high temperatures, we performed QMD simulations of the sulfidation of a reduced MoO_3 flake using S_2 gas molecules at 4500 K (Figure 3a). Detailed information on QMD methods and simulation schedules can be found in the Supporting Information. Our RMD simulations using reactive force fields for CVD process confirm the reaction mechanism for Mo−S bond formation and the evolution of SO molecular fragments deduced from QMD simulations, thus validating our ReaxFF reactive force-field-based RMD simulations.

The reduced MoO_3 flake was vaporized and interacted actively with S_2 gas molecules at 2.0 ps (Figure 3b). Then, the atomistic reaction pathways were investigated using further QMD trajectories up to 2.3 ps (Figure 3c): at 2.0 ps, the S_2 molecule diffused to an O-termination site of the reduced MoO_3 cluster; at 2.1 ps, one of the S atoms in the S_2 molecule chemisorbed nondissociatively onto the O-termination site; at 2.2 ps, the other S atom in the S_2 molecule bound to an undercoordinated Mo atom that was available; at 2.3 ps, finally, the S−S bond broke, resulting in the formation of an SO molecule and Mo−S bond. Comparing the RMD simulations with the QMD trajectories, we confirmed that the reaction mechanism for the sulfidation step of the reduced MoO_3 surface by the RMD simulations was qualitatively consistent with that of our QMD simulations. Furthermore, our proposed reaction mechanism agrees with that of a previous study[18] as follows

$$MoO_3 + 2S \rightarrow MoO_{3-x}S + SO_x \quad (1)$$

Given the results and observations above, we suggest that CVD synthesis of MoS_2 layers from the direct sulfidation of MoO_3 surface can be achieved by combined reduction and sulfidation steps, forming O_2 and SO_x products and eventually leading to Mo−S bond formation.

3.2. Reduction and Sulfidation Rates of the MoO_3 Surface. To understand reaction kinetics for CVD synthesis of MoS_2 layers, we evaluated the reduction and sulfidation rates of the initial MoO_3 surface up to 5.8 ns (Figure 4). For this analysis, RMD simulations of the sulfidation processes (S_2 flow on the MoO_3 surface) were performed at 3000 K for 2.0 ns, followed by 4000 K for 1.8 ns and 5000 K for 2.0 ns. All gas-phase molecules were purged, and then, 4000 S_2 gas molecules were redistributed at 2.0 and 3.8 ns. By using the two simulation procedures described above (i.e., elevating temperatures and purging gas molecules), we were able to efficiently increase the reaction rates for the reduction and sulfidation processes within a limited time scale (~5.8 ns).

These simulation schedules also allowed us to further describe the reaction events after the system reached the first and second plateaus, corresponding to times t = 1.5−2.0 ns and t = 3.5−3.8 ns, respectively. To validate our simulated models with such a high temperature, we provide some simulation details as follows:

1. To support our proposed reaction mechanisms from high-temperature simulations, we performed additional RMD simulations using the same surface model with lower temperatures in the range of 270−1900 K to clearly determine the initiation temperature for the reactions of the SO/SO_2 and Mo−S bond formation. On the basis of the results in Figure S1, we conclude that the number of S−O bonds rapidly increases around 400 K mainly due to S_2 physisorption on the MoO_3 surface, and then SO_x gas molecules start evolving at 1000 K, leading to Mo−S bonds. Moreover, we observed that essential reaction steps at low temperatures are consistent with those in high-temperature simulations, suggesting that it is feasible to simulate critical reactions associated with CVD synthesis at low temperatures although this requires a significant amount of computational costs.
2. To stabilize the MoO_3 surface at 5000 K in our RMD simulations, we have used a one-body spring force on Mo atoms, thus allowing for stable initial and intermediate surface structures.
3. S_2 gas molecules reacting with both sides of MoO_3 are different from the case of experimentally predeposited MoO_3 on the substrate. However, in our previous work

DOI: 10.1021/acs.jpcc.7b12035
J. Phys. Chem. C 2018, 122, 7494−7503

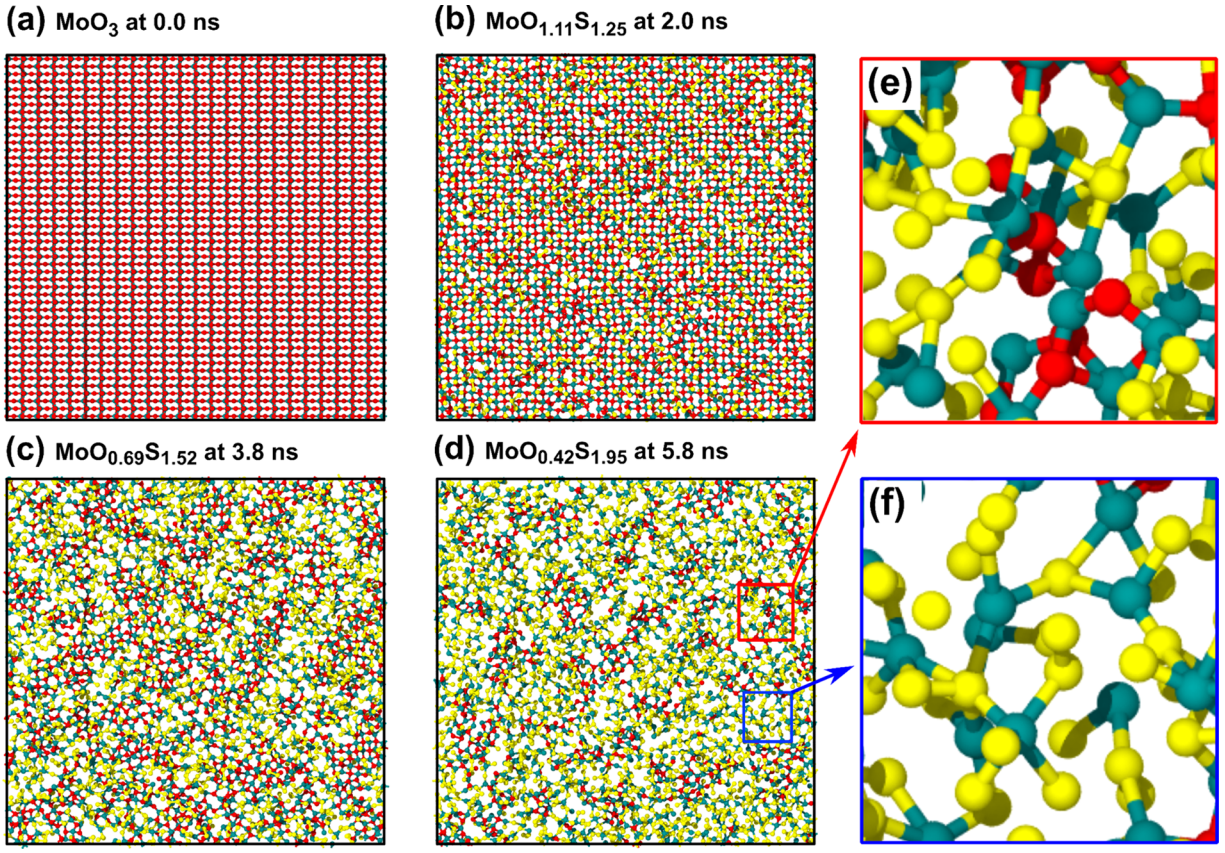

Figure 5. (a–d) Top views of the transformation of MoO_xS_y surface structures in the x–y plane at 0.0, 2.0, 3.8, and 5.8 ns, respectively, corresponding to the time steps in Figure 4. All gas-phase molecules are not shown for clarity. (e, f) Closeups of local surface regions in (d), corresponding to Mo-oxysulfide and MoS_x surface regions, respectively. Note that the initial MoO_3 surface was locally reduced and sulfidized as the simulation time elapsed, thus forming the two local surface regions nonuniformly (red balls and sticks: O; yellow balls and sticks: S; cyan balls and sticks: Mo).

(ref 41), we sulfidized predeposited MoO_3 on the alumina substrate and we still observed the reactions occurring on the MoO_3 surface.

As shown in Figure 4, at the first stage (T = 3,000 K), a fraction of O atoms (red curve) decreased, whereas a fraction of S atoms (yellow curve) increased, after which the system reached the first plateau, indicating that the reduction and sulfidation processes began simultaneously. However, the rate of the reduction process was faster than that of the sulfidation process (e.g., the initial MoO_3 surface converted to $MoO_{1.11}S_{1.25}$ at 2.0 ns). These results reveal that during this stage, the as-deposited MoO_3 surface primarily lost O atoms through the formation of O_2 and SO, leaving unsaturated Mo sites, and the reduced MoO_x surface gained S atoms through reactions of the unsaturated Mo sites and S_2 gas correspondingly (see the previous section for the reaction mechanisms in detail). Movie S1 in the Supporting Information provides full dynamics of the reduction and sulfidation processes up to 2.0 ns.

During the second stage (T = 4,000 K), the reduced $MoO_{1.1}S_{1.25}$ surface (2.0 ns) further transformed into an $MoO_{0.69}S_{1.52}$ surface at 3.8 ns, indicating that the loss of O atoms was still greater than the gain of S atoms, but the reduction and sulfidation rates decreased compared to those in the previous stage up to 2.0 ns. On the basis of these observations, one can expect that as the CVD process proceeded, the O-termination sites that were available on the MoO_xS_y surface gradually decreased because of O_2/SO gas formation (as discussed in the previous section), thus lowering the reduction and sulfidation rates accordingly. These results validate an experimental study[16] reporting that the O-termination site on the MoO_3 surface was the most reactive site for the general sulfidation process.

The $MoO_{0.69}S_{1.52}$ surface (3.8 ns) finally transformed into the $MoO_{0.42}S_{1.95}$ surface at 5.8 ns (T = 5,000 K). During this stage, the reduction and sulfidation rates dropped further, but interestingly, the sulfidation rate was faster than the reduction rate. This can be explained by the fact that more sulfur precursors could actively react with the MoO_xS_y surface because the initial MoO_3 surface was almost reduced ($MoO_{0.69}S_{1.52}$) during the first two stages, and thus, the sulfidation process could predominate as the unsaturated Mo sites provided preferable binding sites for S_2 molecules. In summary, our RMD simulations clarify the reduction and sulfidation kinetics on the MoO_3 surface as follows.

The reduction process is more active than the sulfidation process at the early stage, whereas this trend reverses at the later stage of the CVD process as a result of changes in the reactive sites that are available (the O-termination sites or unsaturated Mo sites) for S_2 precursors. Transformation of the MoO_3 surface to the MoO_xS_y surface was further investigated during the entire CVD process up to 5.8 ps. Figure 5a–d shows the top views (in the x–y plane) of the MoO_xS_y surfaces at 0.0, 2.0, 3.8, and 5.8 ns, respectively, corresponding to the time steps in Figure 4. It is interesting to note that the initial MoO_3

DOI: 10.1021/acs.jpcc.7b12035
J. Phys. Chem. C 2018, 122, 7494–7503

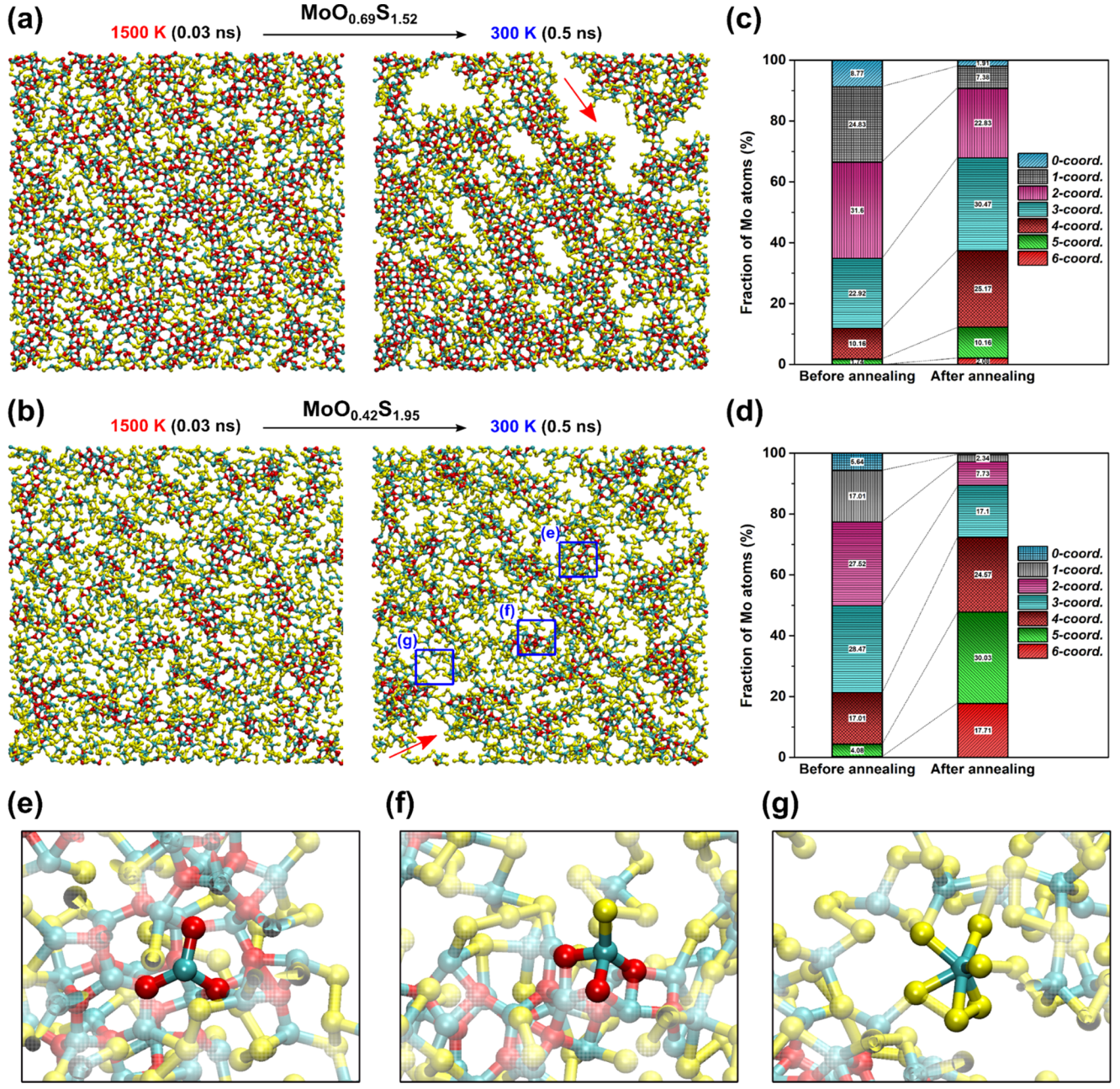

Figure 6. (a, b) Top views of the time evolution of $MoO_{0.69}S_{1.52}$ and $MoO_{0.42}S_{1.95}$ surface morphologies, respectively, during the annealing process. During this process, relatively significant surface voids in the $MoO_{0.69}S_{1.52}$ surface structure were observed, compared to those in the $MoO_{0.42}S_{1.95}$ surface structure. The red arrows in (a, b) point to the largest voids formed during the annealing process. (c, d) Corresponding changes in Mo-coordination numbers, only counted by S atoms, for the $MoO_{0.69}S_{1.52}$ and $MoO_{0.42}S_{1.95}$ surface structures. Note that portions of high Mo-coordination numbers (e.g., 4−6 coordination) increased as the surface structures were locally crystallized. (e−g) Closeups of local surface complexes in the blue rectangles in (b), corresponding to local MoO_x, MoO_xS_y, and MoS_2-like regions, respectively.

surface (Figure 5a) was selectively sulfidized as the simulation time elapsed (Figure 5b−d), and the surface structures were divided primarily into two local regions: Mo-oxysulfide (Figure 5e) and MoS_x (Figure 5f), which were qualitatively consistent with experimental observations.[46] On the basis of our RMD simulations, the characteristics of the local sulfidation can be understood as follows: the reduction process occurred locally on the initial MoO_3 surface, resulting in a wide range of Mo-coordination numbers on the MoO_xS_y surface. This result yielded different sulfidation behaviors on the local MoO_xS_y surface, that is, S_2 molecules reacted preferably with the local MoO_xS_y surface, where a number of Mo-dangling bonds existed.

This trend was also experimentally confirmed by Salazar et al.,[44] reporting that the annealing process for the as-deposited MoO_3 surface generated a wide range of Mo oxidation states, each of which led to different sulfidation rates. Thus, our RMD simulations demonstrated that during the CVD process, the initial MoO_3 surfaces nonuniformly convert into MoO_xS_y surface structures as the surfaces are locally reduced and sulfidized.

3.3. Annealing Process of MoO_xS_y Surfaces. In a typical CVD process, samples are heated and cooled down to room

DOI: 10.1021/acs.jpcc.7b12035
J. Phys. Chem. C 2018, 122, 7494−7503

temperature after the sulfidation process.[47,48] To elucidate the evolution of surface morphologies during this annealing process, we performed RMD simulations of the annealing processes using the $MoO_{0.69}S_{1.52}$ (Figure 5c) and $MoO_{0.42}S_{1.95}$ (Figure 5d) surface structures; all gas-phase molecules were removed from each system, and then, the surface structures were exposed to 1500 K up for 0.25 ns, followed by cooling steps from 1500 to 300 K for 0.25 ns. Figure 6a,b shows the top views of the time evolution of the $MoO_{0.69}S_{1.52}$ and $MoO_{0.42}S_{1.95}$ surface morphologies during the annealing process, respectively. Interestingly, we found that the fractions of O and S atoms on the MoO_xS_y surfaces affected the crystallization behaviors of the surface structures further. Namely, local surface voids were increasingly formed on both surface structures during the annealing process, but relatively large voids were created on the $MoO_{0.69}S_{1.52}$ surface, compared to that on the $MoO_{0.42}S_{1.95}$ surface (see red arrows in Figure 6a,b pointing at the largest surface void on each surface). These results imply that the MoO_xS_y surface with sulfur deficiency ($MoO_{0.69}S_{1.52}$) induces Mo atoms to further diffuse into neighboring S atoms that are available during the crystallization stage. In contrast, the MoO_xS_y surface with sufficient sulfur ($MoO_{0.42}S_{1.95}$) allowed relatively little diffusion of Mo atoms on the surface, resulting in reduced surface voids on its surface structure accordingly. Such void formation, depending on the amount of gas-phase sulfur precursors, was also observed experimentally by Taheri et al.[20] using optical microscope images. Thus, it is expected that the degree to which Mo atoms diffuse, affected by the fraction of S atoms on the surface, is responsible for the size of surface voids that are formed on the MoO_xS_y samples during the local crystallization step. Full dynamics of the local void formation on the $MoO_{0.69}S_{1.52}$ and $MoO_{0.42}S_{1.95}$ surface structures are available in Movies S2 and S3 (the Supporting Information), respectively. The initial thickness of the MoO_3 surface (i.e., O−O distance within a single MoO_3 layer) was 6.74 Å. The single MoO_3 layer was cleaved from the bulk α-MoO_3 crystal in the z-direction. After sulfidation and annealing processes (the right snapshot in Figure 6a), the average thickness was between 4.2 and 4.8 Å (see Figure S2 in the Supporting Information for the side views of the surface models during RMD simulations). The thickness of the intermediate MoO_xS_y surface was measured from S−S bond distances in the local MoS_2-like complexes, which can be primarily considered as real hexagonal MoS_2 structures. As the surface becomes sulfidized, the thickness of the initial single layer decreases. Such a thickness change could be understood by the fact that the initial MoO_3 surface has double sheets of Mo planes with O-termination sites on the top and bottom surfaces,[49] whereas the MoS_2 monolayer consists of a single Mo plane with S atoms on the top and bottom surfaces.[50] Our RMD simulations reveal that as the O atoms in the MoO_3 surface were replaced by S atoms, the Mo atoms get redistributed (i.e., they form a single plane), and thus, the intermediate structures became thinner during sulfidation.

Additionally, changes in Mo-coordination numbers (only counted by the surrounding S atoms) were measured to study local coordination complexes on the MoO_xS_y surface. Figure 6c,d compares the changes in Mo-coordination numbers of the $MoO_{0.69}S_{1.52}$ surface to that on the $MoO_{0.42}S_{1.95}$ surface. It is worth noting that after the annealing process, the MoO_xS_y surface with sufficient sulfur led to an increased portion of highly coordinated (4-, 5-, and 6-coordination) local complexes (72.3%), whereas a relatively small portion of high Mo-coordination numbers (38.4%) was found on the MoO_xS_y surface with sulfur deficiency. These results suggest that sufficient sulfur ingredients are required to form highly crystallized MoS_2 layers.

Subsequently, three types of local surface complexes were found: MoO_x, MoO_xS_y, and MoS_2-like surface complexes, as shown in Figure 6e−g, respectively. The observations of these three clusters were qualitatively consistent with those of Salazar et al.[44] They also reported that after CVD growth, a stable MoS_2 structure contained a small amount of Mo-oxide and Mo-oxysulfide intermediates, which could render the MoS_2 layers nonuniform. We further elucidate in this work that these structures can be controlled by altering the duration of sulfur exposure to the MoO_xS_y surface. As such, it can be assumed that a large portion of local MoS_2-like clusters and small portions of local MoO_x or MoO_xS_y clusters are responsible for high-quality MoS_2 samples. To confirm this prediction, the percentage of local surface complexes on the $MoO_{0.69}S_{1.52}$ and $MoO_{0.42}S_{1.95}$ surfaces was measured after the annealing process (Table 1).

Table 1. Comparison of Local Surface Complexes (MoO_x, MoO_xS_y, and MoS_2-like Surface Complexes, Indicated in Figure 6e−g) in the Annealed $MoO_{0.69}S_{1.52}$ and $MoO_{0.42}S_{1.95}$ Surface Structures[a]

annealed surface composition	percentage of local surface compounds		
	MoO_x cluster (%)	MoO_xS_y cluster (%)	MoS_2-like cluster (%)
$MoO_{0.69}S_{1.52}$	1.91	96.35	1.74
$MoO_{0.42}S_{1.95}$	0.52	77.78	21.70

[a]Note that the lower oxygen and higher sulfur components in the surface structures lead to a higher portion of local MoS_2-like clusters and smaller surface voids, as shown in Figure 6b.

As expected, the $MoO_{0.42}S_{1.95}$ (sulfur-sufficient) surface structures, corresponding to Figure 6b, contained a relatively large fraction of MoS_2-like surface complexes (21.70%) and smaller fractions of MoO_xS_y (77.78%) and MoO_x (0.52%) surface complexes, when compared to those on the $MoO_{0.69}S_{1.52}$ (sulfur-deficient) surface structure (i.e., MoS_2-like: 1.74%; MoO_xS_y: 96.35%; MoO_x: 1.91%). The structure of MoS_2 monolayer consists of a single sheet of Mo plane sandwiched between two planes of S atoms, thus forming a hexagonal crystal structure. During our simulations, MoS_2-like structures in Figure 6g were found to be qualitatively consistent with the local hexagonal structures in MoS_2 monolayers as each Mo atom in the MoS_2 structure possesses six neighboring S atoms on it. This can be supported by changes in the number of neighboring S atoms on Mo elements in Figure 6c,d. On the basis of this structural information, the intermediate surface structure, derived by our RMD simulations, could be further converted into local hexagonal MoS_2 structures, and they are expected to be merged into a single crystalline MoS_2 layer during the long-time introduction of sulfur precursors, which has been postponed for a future work.

4. CONCLUSIONS

In conclusion, we performed RMD simulations of the direct sulfidation of monolayered MoO_3 surface using gas-phase S_2 precursors to investigate atomic-scale reaction processes for CVD synthesis of MoS_2 layers. Our RMD simulations, validated by our QMD simulations and data from the experimental

DOI: 10.1021/acs.jpcc.7b12035
J. Phys. Chem. C 2018, 122, 7494−7503

literature, revealed the detailed reaction mechanisms and growth kinetics for the direct sulfidation of the MoO_3 surface as follows: (1) the reduction and sulfidation processes primarily begin from the O-termination sites, forming O_2/SO gas molecules and consequently Mo−S bond; (2) the initial MoO_3 surface is locally (nonuniformly) reduced and sulfidized, depending on the available reactive sites, like the O-termination and unsaturated Mo sites; and (3) the fraction of S atoms on the MoO_xS_y surface influences the degree of void formation and Mo-coordination changes, as well as the portion of the local coordination complexes. Owing to the limited length of molecular dynamics trajectories, we were unable to simulate the full dynamics of conversion of MoO_3 to MoS_2 structure in this work. Therefore, the initial MoO_3 surface structures were not completely converted to MoS_2 stoichiometric structures at the end of our RMD simulations. We plan to perform long-time RMD simulations (e.g., t > 100 ns) to further clarify the formation of crystalline hexagonal MoS_2 structures during CVD synthesis of MoS_2 layers. To implement these long reactive simulations for times that are in ∼100 ns time regime and beyond, we have developed new time-to-solution algorithms that allow us to distribute our simulations on a much larger number of cores than is possible in conventional domain decomposition algorithms.

Our new chemical insights allow us to further clarify key reaction events during the CVD process, including the role of O-termination in the reduction/sulfidation steps and the origin of experimentally observed discontinuities and nonuniformities on the MoO_xS_y samples.[20,51,52] We believe that our work will help guide scalable CVD techniques for the synthesis of large-scale and defect-free MoS_2 layers and other layered TMDC materials for future applications.

■ ASSOCIATED CONTENT

Supporting Information

The Supporting Information is available free of charge on the ACS Publications website at DOI: 10.1021/acs.jpcc.7b12035.

Details of QMD methods and simulations schedules; validation of RMD simulations; changes in the thickness of surface structures during the sulfidation process (PDF)

ReaxFF reactive force-field parameters for Mo/O/S elements (PDF)

RMD trajectories of the reduction and sulfidation processes up to 2.0 ns (Movie S1); RMD trajectories of the local void formation on the $MoO_{0.69}S_{1.52}$ surface during the annealing process (Movie S2); RMD trajectories of the local void formation on the $MoO_{0.42}S_{1.95}$ surface during the annealing process (Movie S3) (ZIP)

■ AUTHOR INFORMATION

Corresponding Author

*E-mail: priyav@usc.edu.

ORCID

Sungwook Hong: 0000-0003-3569-7701

Aravind Krishnamoorthy: 0000-0001-6778-2471

Aiichiro Nakano: 0000-0003-3228-3896

Priya Vashishta: 0000-0003-4683-429X

Notes

The authors declare no competing financial interest.

■ ACKNOWLEDGMENTS

This work was supported as part of the Computational Materials Sciences Program funded by the U.S. Department of Energy, Office of Science, Basic Energy Sciences, under Award Number DE-SC00014607. The simulations were performed at the Argonne Leadership Computing Facility under the DOE INCITE program and at the Center for High Performance Computing of the University of Southern California.

■ ABBREVIATIONS

TMDC, Transition metal dichalcogenide; RMD, Reactive molecular dynamics; QMD, Quantum molecular dynamics; CVD, Chemical vapor deposition

■ REFERENCES

(1) Geim, A. K.; Grigorieva, I. V. Van der Waals Heterostructures. *Nature* **2013**, *499*, 419−425.

(2) Chen, Y.; et al. Ultra-Fast Self-Assembly and Stabilization of Reactive Nanoparticles in Reduced Graphene Oxide Films. *Nat. Commun.* **2016**, *7*, No. 12332.

(3) Sabourin, J. L.; Dabbs, D. M.; Yetter, R. A.; Dryer, F. L.; Aksay, I. A. Functionalized Graphene Sheet Colloids for Enhanced Fuel/Propellant Combustion. *ACS Nano* **2009**, *3*, 3945−3954.

(4) Mak, K. F.; Lee, C.; Hone, J.; Shan, J.; Heinz, T. F. Atomically Thin MoS_2: A New Direct-Gap Semiconductor. *Phys. Rev. Lett.* **2010**, *105*, No. 136805.

(5) Lembke, D.; Kis, A. Breakdown of High-Performance Monolayer MoS_2 Transistors. *ACS Nano* **2012**, *6*, 10070−10075.

(6) Schmidt, H.; Wang, S.; Chu, L.; Toh, M.; Kumar, R.; Zhao, W.; Castro Neto, A.; Martin, J.; Adam, S.; Özyilmaz, B.; et al. Transport Properties of Monolayer MoS_2 Grown by Chemical Vapor Deposition. *Nano Lett.* **2014**, *14*, 1909−1913.

(7) Wang, Q. H.; Kalantar-Zadeh, K.; Kis, A.; Coleman, J. N.; Strano, M. S. Electronics and Optoelectronics of Two-Dimensional Transition Metal Dichalcogenides. *Nat. Nanotechnol.* **2012**, *7*, 699−712.

(8) Nourbakhsh, A.; Zubair, A.; Sajjad, R. N.; Tavakkoli KG, A.; Chen, W.; Fang, S.; Ling, X.; Kong, J.; Dresselhaus, M. S.; Kaxiras, E.; et al. MoS_2 Field-Effect Transistor with Sub-10 nm Channel Length. *Nano Lett.* **2016**, *16*, 7798−7806.

(9) Dong, L.; Wang, J.; Namburu, R.; O'Regan, T. P.; Dubey, M.; Dongare, A. M. Edge Effects on Band Gap Energy in Bilayer 2H-MoS_2 under Uniaxial Strain. *J. Appl. Phys.* **2015**, *117*, No. 244303.

(10) Ganatra, R.; Zhang, Q. Few-Layer MoS_2: A Promising Layered Semiconductor. *ACS Nano* **2014**, *8*, 4074−4099.

(11) Venkata Subbaiah, Y.; Saji, K.; Tiwari, A. Atomically Thin MoS_2: A Versatile Nongraphene 2D Material. *Adv. Funct. Mater.* **2016**, *26*, 2046−2069.

(12) Lee, Y.-H.; Zhang, X. Q.; Zhang, W.; Chang, M. T.; Lin, C. T.; Chang, K. D.; Yu, Y. C.; Wang, J. T. W.; Chang, C. S.; Li, L. J.; et al. Synthesis of Large-Area MoS_2 Atomic Layers with Chemical Vapor Deposition. *Adv. Mater.* **2012**, *24*, 2320−2325.

(13) Chen, J.; Tang, W.; Tian, B.; Liu, B.; Zhao, X.; Liu, Y.; Ren, T.; Liu, W.; Geng, D.; Jeong, H. Y.; et al. Chemical Vapor Deposition of High-Quality Large-Sized MoS_2 Crystals on Silicon Dioxide Substrates. *Adv. Sci.* **2016**, *3*, No. 1500033.

(14) van der Zande, A. M.; Huang, P. Y.; Chenet, D. A.; Berkelbach, T. C.; You, Y.; Lee, G.-H.; Heinz, T. F.; Reichman, D. R.; Muller, D. A.; Hone, J. C. Grains and Grain Boundaries in Highly Crystalline Monolayer Molybdenum Disulphide. *Nat. Mater.* **2013**, *12*, 554−561.

(15) Najmaei, S.; Liu, Z.; Zhou, W.; Zou, X.; Shi, G.; Lei, S.; Yakobson, B. I.; Idrobo, J.-C.; Ajayan, P. M.; Lou, J. Vapor Phase Growth and Grain Boundary Structure of Molybdenum Disulfide Atomic Layers. *Nat. Mater.* **2013**, *12*, 754−759.

(16) Weber, T.; Muijsers, J.; Van Wolput, J.; Verhagen, C.; Niemantsverdriet, J. Basic Reaction Steps in the Sulfidation of Crystalline MoO_3 to MoS_2, as Studied by X-Ray Photoelectron and

DOI: 10.1021/acs.jpcc.7b12035
J. Phys. Chem. C 2018, 122, 7494−7503

Infrared Emission Spectroscopy. *J. Phys. Chem.* **1996**, *100*, 14144−14150.
(17) Kumar, P.; Singh, M.; Sharma, R. K.; Reddy, G. Reaction Mechanism of Core−Shell MoO_2/MoS_2 Nanoflakes Via Plasma-Assisted Sulfurization of MoO_3. *Mater. Res. Express* **2016**, *3*, No. 055021.
(18) Jeon, J.; Lee, J.; Yoo, G.; Park, J.-H.; Yeom, G. Y.; Jang, Y. H.; Lee, S. Size-Tunable Synthesis of Monolayer MoS_2 Nanoparticles and Their Applications in Non-Volatile Memory Devices. *Nanoscale* **2016**, *8*, 16995−17003.
(19) Albiter, M. A.; Huirache-Acuna, R.; Paraguay-Delgado, F.; Rico, J.; Alonso-Nunez, G. Synthesis of MoS_2 Nanorods and Their Catalytic Test in the HDS of Dibenzothiophene. *Nanotechnology* **2006**, *17*, No. 3473.
(20) Taheri, P.; Wang, J.; Xing, H.; Destino, J. F.; Arik, M. M.; Zhao, C.; Kang, K.; Blizzard, B.; Zhang, L.; Zhao, P.; et al. Growth Mechanism of Largescale MoS_2 Monolayer by Sulfurization of MoO_3 Film. *Mater. Res. Express* **2016**, *3*, No. 075009.
(21) Lin, Y.-C.; Zhang, W.; Huang, J.-K.; Liu, K.-K.; Lee, Y.-H.; Liang, C.-T.; Chu, C.-W.; Li, L.-J. Wafer-Scale MoS_2 Thin Layers Prepared by MoO_3 Sulfurization. *Nanoscale* **2012**, *4*, 6637−6641.
(22) van Duin, A. C. T.; Verners, O.; Shin, Y.-K. Reactive Force Fields: Concepts of Reaxff and Applications to High-Energy Materials. *Int. J. Energ. Mater. Chem. Propul.* **2013**, *12*, 95−118.
(23) Manikandan, P.; Carter, J. A.; Dlott, D. D.; Hase, W. L. Effect of Carbon Chain Length on the Dynamics of Heat Transfer at a Gold/Hydrocarbon Interface: Comparison of Simulation with Experiment. *J. Phys. Chem. C* **2011**, *115*, 9622−9628.
(24) Klein, M. L.; Shinoda, W. Large-Scale Molecular Dynamics Simulations of Self-Assembling Systems. *Science* **2008**, *321*, 798−800.
(25) Mo, Y.; Turner, K. T.; Szlufarska, I. Friction Laws at the Nanoscale. *Nature* **2009**, *457*, 1116−1119.
(26) Sinnott, S. B.; Brenner, D. W. Three Decades of Many-Body Potentials in Materials Research. *MRS Bull.* **2012**, *37*, 469−473.
(27) Russo, M. F.; van Duin, A. C. Atomistic-Scale Simulations of Chemical Reactions: Bridging from Quantum Chemistry to Engineering. *Nucl. Instrum. Methods Phys. Res., Sect. B* **2011**, *269*, 1549−1554.
(28) van Duin, A. C. T.; Dasgupta, S.; Lorant, F.; Goddard, W. A. Reaxff: A Reactive Force Field for Hydrocarbons. *J. Phys. Chem. A* **2001**, *105*, 9396−9409.
(29) Shan, T.-R.; Devine, B. D.; Hawkins, J. M.; Asthagiri, A.; Phillpot, S. R.; Sinnott, S. B. Second-Generation Charge-Optimized Many-Body Potential for Si/SiO_2 and Amorphous Silica. *Phys. Rev. B* **2010**, *82*, No. 235302.
(30) Liang, T.; Devine, B.; Phillpot, S. R.; Sinnott, S. B. Variable Charge Reactive Potential for Hydrocarbons to Simulate Organic-Copper Interactions. *J. Phys. Chem. A* **2012**, *116*, 7976−7991.
(31) Liang, T.; Shin, Y. K.; Cheng, Y.-T.; Yilmaz, D. E.; Vishnu, K. G.; Verners, O.; Zou, C.; Phillpot, S. R.; Sinnott, S. B.; van Duin, A. C. T. Reactive Potentials for Advanced Atomistic Simulations. *Annu. Rev. Mater. Res.* **2013**, *43*, 109−129.
(32) Goddard, W. A., III; van Duin, A. C. T.; Chenoweth, K.; Cheng, M.-J.; Pudar, S.; Oxgaard, J.; Merinov, B.; Jang, Y. H.; Persson, P. Development of the Reaxff Reactive Force Field for Mechanistic Studies of Catalytic Selective Oxidation Processes on $BiMoO_X$. *Top. Catal.* **2006**, *38*, 93−103.
(33) Vasenkov, A.; Newsome, D.; Verners, O.; Russo, M. F., Jr.; Zaharieva, R.; van Duin, A. C. Reactive Molecular Dynamics Study of Mo-Based Alloys under High-Pressure, High-Temperature Conditions. *J. Appl. Phys.* **2012**, *112*, No. 013511.
(34) Hong, S.; van Duin, A. C. Atomistic-Scale Analysis of Carbon Coating and Its Effect on the Oxidation of Aluminum Nanoparticles by Reaxff-Molecular Dynamics Simulations. *J. Phys. Chem. C* **2016**, *120*, 9464−9474.
(35) Jack, R.; Sen, D.; Buehler, M. J. Graphene Nanocutting through Nanopatterned Vacancy Defects. *J. Comput. Theor. Nanosci.* **2010**, *7*, 354−359.
(36) Cranford, S.; Buehler, M. J. Twisted and Coiled Ultralong Multilayer Graphene Ribbons. *Modell. Simul. Mater. Sci. Eng.* **2011**, *19*, 054003.
(37) Ostadhossein, A.; Rahnamoun, A.; Wang, Y.; Zhao, P.; Zhang, S.; Crespi, V. H.; van Duin, A. C. T. Reaxff Reactive Force-Field Study of Molybdenum Disulfide (MoS_2). *J. Phys. Chem. Lett.* **2017**, *8*, 631−640.
(38) Onofrio, N.; Guzman, D.; Strachan, A. The Dynamics of Copper Intercalated Molybdenum Ditelluride. *J. Chem. Phys.* **2016**, *145*, No. 194702.
(39) Yoon, K.; Rahnamoun, A.; Swett, J. L.; Iberi, V.; Cullen, D. A.; Vlassiouk, I. V.; Belianinov, A.; Jesse, S.; Sang, X.; Ovchinnikova, O. S.; et al. Atomistic-Scale Simulations of Defect Formation in Graphene under Noble Gas Ion Irradiation. *ACS Nano* **2016**, *10*, 8376−8384.
(40) Senftle, T. P.; et al. The Reaxff Reactive Force-Field: Development, Applications and Future Directions. *npj Comput. Mater.* **2016**, *2*, No. 15011.
(41) Hong, S.; Krishnamoorthy, A.; Rajak, P.; Tiwari, S. C.; Misawa, M.; Shimojo, F.; Kalia, R. K.; Nakano, A.; Vashishta, P. Computational Synthesis of MoS_2 Layers by Reactive Molecular Dynamics Simulations: Initial Sulfidation of MoO_3 Surfaces. *Nano Lett.* **2017**, *17*, 4866−4872.
(42) Nosé, S. A Unified Formulation of the Constant Temperature Molecular Dynamics Methods. *J. Chem. Phys.* **1984**, *81*, 511−519.
(43) Hoover, W. G. Canonical Dynamics: Equilibrium Phase-Space Distributions. *Phys. Rev. A* **1985**, *31*, 1695−1697.
(44) Salazar, N.; Beinik, I.; Lauritsen, J. V. Single-Layer MoS_2 Formation by Sulfidation of Molybdenum Oxides in Different Oxidation States on Au (111). *Phys. Chem. Chem. Phys.* **2017**, *19*, 14020−14029.
(45) Li, X. L.; Li, Y. D. Formation of MoS_2 Inorganic Fullerenes (Ifs) by the Reaction of MoO_3 Nanobelts and S. *Chem. - Eur. J.* **2003**, *9*, 2726−2731.
(46) Zhu, D.; Shu, H.; Jiang, F.; Lv, D.; Asokan, V.; Omar, O.; Yuan, J.; Zhang, Z.; Jin, C. Capture the Growth Kinetics of CVD Growth of Two-Dimensional MoS_2. *npj 2D Mater. Appl.* **2016**, *1*, No. 8.
(47) Liu, X.; Balla, I.; Bergeron, H.; Campbell, G. P.; Bedzyk, M. J.; Hersam, M. C. Rotationally Commensurate Growth of MoS_2 on Epitaxial Graphene. *ACS Nano* **2016**, *10*, 1067−1075.
(48) Sun, L.; Leong, W. S.; Yang, S.; Chisholm, M. F.; Liang, S. J.; Ang, L. K.; Tang, Y.; Mao, Y.; Kong, J.; Yang, H. Y. Concurrent Synthesis of High-Performance Monolayer Transition Metal Disulfides. *Adv. Funct. Mater.* **2017**, *27*, No. 1605896.
(49) Liu, D.; Lei, W.; Hao, J.; Liu, D.; Liu, B.; Wang, X.; Chen, X.; Cui, Q.; Zou, G.; Liu, J.; et al. High-Pressure Raman Scattering and X-Ray Diffraction of Phase Transitions in MoO_3. *J. Appl. Phys.* **2009**, *105*, No. 023513.
(50) Cao, T.; Wang, G.; Han, W.; Ye, H.; Zhu, C.; Shi, J.; Niu, Q.; Tan, P.; Wang, E.; Liu, B.; et al. Valley-Selective Circular Dichroism of Monolayer Molybdenum Disulphide. *Nat. Commun.* **2012**, *3*, No. 887.
(51) Murr, L.; Berry, V. The Nature of Microstructural Voids and Occlusion-Like Contrast Phenomena in MoS_2. *Metallography* **1975**, *8*, 337−341.
(52) Zou, X.; Wang, J.; Chiu, C. H.; Wu, Y.; Xiao, X.; Jiang, C.; Wu, W. W.; Mai, L.; Chen, T.; Li, J.; et al. Interface Engineering for High-Performance Top-Gated MoS_2 Field-Effect Transistors. *Adv. Mater.* **2014**, *26*, 6255−6261.

DOI: 10.1021/acs.jpcc.7b12035
J. Phys. Chem. C 2018, 122, 7494−7503